Heliyon 8 (2022) e12610

Contents lists available at ScienceDirect

Heliyon

journal homepage: www.cell.com/heliyon

Research article

Photocatalytic remediation of methylene blue using hydrothermally synthesized H-Titania and Na-Titania nanotubes

Aderemi Timothy Adeleye [a,b], Kingsley Igenepo John [b,c,d], Joshua O. Ighalo [e,f], Samuel Ogunniyi [e], Comfort Abidemi Adeyanju [e], Adewale George Adeniyi [e], Mohammed Elawad [g,**], Martins O. Omorogie [h,i,*]

[a] Global Centre for Environmental Remediation (GCER), The University of Newcastle, Callaghan, Australia
[b] Organization of African Academic Doctor (OAAD), Off Kamiti Road, P. O. Box 25305000100, Nairobi, Kenya
[c] College of Science, Health, Engineering and Education, Murdoch University, Murdoch 6150, Australia
[d] Department of Pure and Applied Chemistry, College of Natural and Applied Sciences, Veritas University, P.M.B. 5171, Abuja, Nigeria
[e] Department of Chemical Engineering, University of Ilorin, P. M. B. 1515, Ilorin, Nigeria
[f] Department of Chemical Engineering, Nnamdi Azikiwe University, P. M. B. 5025, Awka, Nigeria
[g] Faculty of Materials and Chemical Engineering, Yibin University, 64400, Yibin, China
[h] Department of Chemical Sciences, Redeemer's University, P.M.B. 230, Ede, 232101, Nigeria
[i] Environmental Science and Technology Unit, African Centre of Excellence for Water and Environmental Research (ACEWATER), Redeemer's University, P.M.B. 230, Ede, 232101, Nigeria

ARTICLE INFO

Keywords:
Environmental protection
Methylene blue
Photocatalytic degradation
Titania

ABSTRACT

Although nanotube is among the most effective morphology of Titania due to its unilateral pathway for photo-generated charge transfer and mechanical stability, its performance is still hampered by high recombination. In the present study, to further improve the photocatalytic degradation performance of Titania, univalent elements of H and Na were respectively ion-exchanged into the Titania nanotubes (TNTs). The photocatalyst was characterized using XRD, TEM, ICP-AES, and FTIR. The modified samples displayed enhanced photocatalytic degradation performance over Degussa TiO_2 under UV-A light illumination of MB. The rate constants of NaTNT and HTNT were 16 and 13 times that of Degussa TiO_2. Specifically, the Na-TNTs showed better photocatalytic degradation activity than H-TNTs with a rate constant of 0.12 min^{-1} while the latter showed 0.09 min^{-1}. The optimum adsorption and photocatalytic performance of NaTNT were determined at pH 6 achieving about 99% MB removal within 10 min of irradiation. The ion exchange NaTNT displayed excellent reusability after the fifth cycle of the photocatalytic tests and superoxide radicals were experimentally determined to be the main reactive oxygen species involved in the photocatalytic degradation of MB.

1. Introduction

Clean water is progressively scarce owing to increased pollution of the existing water sources particularly due to discharge of various contaminants [1]. Pollution is one of global environmental issues caused by hazardous substances. Common sources of environmental degradation include mining, smelting, textile industry and electronic waste disposal, and agricultural activities (pesticides and fertilisers) [2]. Dyes are organic contaminants which when released into the environment have potential to endanger both living organisms on land and under water [3]. Various organic contaminants such as pharmaceutical [2, 4], plastic, textile [5], paint [6], fungicide [7] and cosmetic are being discharged directly from the manufacturers into the source of water bodies [2, 5]. The release of organic pollutants and other carcinogenic petrochemicals have been a great concern among chemical engineers and environmentalists [5, 7]. Pollutants released from industrial wastewater are a crucial environmental concern with grave consequences on humans, environment and economic prospects [5, 8].

The removal of dye from contaminated waters is an essential task to safeguard the ecosystems and humans towards realization of eco-friendliness and sustainability of the environment [9]. The chemical compositions of most of the existing dyes are somewhat complicated and

* Corresponding author.
** Corresponding author.
E-mail addresses: mohammed.toum@yahoo.com, 2020100003@yibinu.edu.cn (M. Elawad), omorogiem@run.edu.ng, mo.omorogie@tum.de (M.O. Omorogie).

https://doi.org/10.1016/j.heliyon.2022.e12610
Received 4 August 2022; Received in revised form 10 October 2022; Accepted 16 December 2022

this makes them defiant to aerobic digestion and, however, they are so stable when subjected to light, oxidising agents and heat [10]. Methylene blue (MB) is one of the commonly used dyes for dyeing cotton, silk, and wood [9, 10]. A high concentration of the dye in the water bodies has been related to the wastewater emitted from major manufacturing industries [10]. MB is a cationic dye exhibiting various uses in dyeing industries [11]. These advancements signify that the existence of dyes in the water bodies is undesirable, obnoxious and detrimental to human health together with flora and fauna [12].

Therefore, there is need to develop environmental remediation technology to eliminate these hazardous materials [9, 10, 13, 14]. Different methods such as heterogeneous catalytic oxidation with H_2O_2 [15], heterogeneous photocatalytic process [16], electrochemical oxidation [17], Fenton/photo-Fenton oxidation [16, 17], ozonation [18], biodegradation [19], chlorination [20, 21], combined flocculation/coagulation [22], adsorption [4, 8], reverse osmosis [23] and UV/H_2O_2 treatment can be used to obliterate organic pollutants [24].

Currently, among the advanced oxidation processes (AOPs), photocatalysis reactions is a promising and one of the suitable techniques for the clean-up from textile wastewater discharge due to their efficiency [5], low maintenance [17] and long-term applicability [3]. The treatment of pollutants is done with the aid of sunlight for the decomposition of organic contaminants [3, 16]. The key to the exploitation of photocatalytic technology is efficient utilisation of photocatalytic materials [3, 16, 17]. The photodegradation processes become more cost-effective if sunlight is consumed instead of ultraviolet light [16]. Degradation of organic pollutants has also produced great importance for its potential to remove the hazardous chemical substances present in water [3, 17].

During photocatalytic reaction, electron hole pairs are generated as a result of semiconductor being exposed to light radiation [16]. During this process electrons move the region of conduction band (CB) and this result to the formation of hole in the region of valence band (VB) through oxidation and reduction process. Consequently, photocatalytic material needs to be photoactive in order to attract the required solar radiation, stable, harmless and cost-effective [3]. In the last few decades, TiO_2 has been employed as exceptional photocatalytic materials because of its strong oxidising power, long term thermodynamic constancy and relatively eco-benign in nature [25, 26]. Nevertheless, owing to huge band gap of TiO_2, it expected that ultraviolet light invigorating the photocatalytic material in the process [27]. It was established that the remarkable high surface area-to-volume ratio of titania (TiO_2) nanotubes enhances their absorption characteristic feature and capacity to drive electrochemical reactions [28].

Crystalline forms of TiO_2 are brookite, anatase and rutile. Among these three phases, anatase has been proven to gaining attention owing to its high photoactivity potential [27, 29, 30]. Alkali-based modifications on TiO_2 encourage electron transfer resulting in better electron-hole separation [29, 30]. Nanotube derived materials such as titanium dioxide (TiO_2) nanotubes (TNTs) are incomparable promising nanomaterials for research and have been reportedly employed in numerous applications such as photocatalytic systems, also in sensing application for pH and gases and as an efficient instrument for the environmental application [31, 32].

In the past few years, various techniques have been applied to improve the photocatalytic approach of titanium dioxide for the treatment of water and wastewater such as doping or co-doping with metal [33, 34], or non-metal [33, 35, 36].

Among the various treatment technologies suitable for wastewater, photocatalytic reaction as a heterogeneous advanced oxidation method is considered viable, economical, and in many cases ecological compatible for the elimination of hazardous contaminants or lowering them to acceptable and recommended concentration before wastewater discharge is released into the environment [3, 16]. For instance, the high efficiency of photocatalytic technique applied for the in the degradation of organic contaminants in contaminated water [3]. Photocatalytic system employs catalytic materials for the purpose of irradiation [37]. In the process electrons holes are generated and dissociation occurs which result to the production of efficient active scavenger ions [38, 39]. These resultant scavenger ions cause degradation of the contaminants with the formation of less toxic by-products [39, 40]. The process is chain reaction in nature and occurs repeatedly until complete degradation is achieved with completion in the mineralization of pollutants [38, 40, 41].

In last decades various remediation techniques have applied for the clean-up of contaminated soil and water towards achieving sustainable, eco-friendly, and cleaner ecological sphere. Nanotechnology has been proven to be suitable and equally efficient approach with the use of nano-adsorbents for the remediation of contaminants [42, 43, 44]. In the recent, many TiO_2-derived photocatalytic materials have been developed and employed such as nanorods [45], nanotubes [26, 46, 47], nanofibres [48], nanowires [49]. These nano-derived materials are finding useful applications in the clean-up of the environment due to their interesting characteristic features [47], such as ion-exchange potential and efficient role in photocatalysis [46, 50]. Besides, vulnerable to be tuned or modified via doping or co-doping with metal and/non-metals seems to be another quality that made them suitable for photocatalytic applications [51, 52, 53]. Furthermore, these materials have been synthesized using various methods and utilization of electrochemical oxidation has been reported to monitor the geometrical size of the layer titanate [54].

Among the previously employed preparation techniques for titanate nanotubes (TNTs) includes sol–gel [55], template method [56], hydrothermal treatment [46, 50], anodization process [57]. Among the above-mentioned methods for the synthesis of titanate nanotubes, hydrothermal has been widely employed owing to the simpler procedure and eco-friendliness in nature without further modification of the existing apparatus to suit their current synthesis [46, 50]. Hence, it was applied for the synthesis of titanate nanotubes used as photocatalytic materials in this research.

In this study, photocatalytic degradation reactions with methylene blue (MB) was performed and the effect of ion-exchange of titania nanotubes through photocatalytic degradation activities were investigated. Characterisation of the employed catalytic materials was done using XRD, BET, TEM, ICP-AES, and FTIR. The ion exchanged NaTNT displayed excellent reusability after the fifth cycle of the photocatalytic tests and superoxide radicals were experimentally determined to be the principal reactive oxygen species involved in the degradation of MB with photocatalytic technique. The study was conducted under batch and the data generated were evaluated with various study parameters to determine the efficacies of the nanotubes for the removal of the organic pollutants.

2. Experimental

2.1. Materials and reagents

Commercially procured P25 Degussa Titanium dioxide (P25 TiO_2) (P25, 99.5%) and Methylene blue (MB) (analytical reagent, 99%) were obtained from Shangweikelin Co. Ltd., China and Société Chimique Point Girard, 16, Boulevard du General Leclerc 92115 Clichy France respectively. The maximum absorption was taken to be 664 nm. The stock solution of MB (1000 mg.L^{-1}) was made by the dissolution of 1 g MB powder in 1000 mL of deionised water. Thereafter, the stock solutions of lesser concentrations were made by using the alternative dilution formula. Sodium hydroxide (NaOH) (analytical reagent, 99%) and nitric acid (HNO_3) (analytical reagent, 99%) were purchased from the Damão Chemical Reagent Factory. The deionised water was used throughout the experiment. Reagents used were not subject to extra purification since they are procured as analytical grades.

2.2. Preparation of protonated titanate nanotubes (HTNT) and sodium titanate nanotubes (NaTNT) catalysts

Both NaTNT and HTNT were produced using modified preparation approach previously published [47, 50, 58, 59]. For P25 TiO_2 (Degussa),

5.0 g quantity and commercial grade was dispersed into a 70 mL aqueous solution of 10 M NaOH. After it was rigorously stirred for 30 min at 500 rpm using a magnetic stirrer, the mixture was poured into a 150 mL autoclave container and moved to an oven for hydrothermal treatment while the reaction conditions being kept at 423 K for duration of 20 h. After 20 h, it was subjected to filtration and washing using a large volume of deionised water until the pH of the filtrate is neutral (pH = 7.0). The as-prepared NaTNT was divided into equal parts with first dried overnight at 333 K to obtain the pure NaTNT which was subsequently processed into powder forms. The other part kept was later treated with 0.1 M $HNO_3$and filtered with thorough washing using deionised water, when the filtrate was neutral the white solid product was dried overnight at 333 K to get our HTNT.

Titanium dioxide (TiO_2) designated P25 TiO_2 was equally employed in MB removal studies for comparative study.

Teflon-lined autoclave and a high-temperature furnace were used for the hydrothermal synthesis of the catalysts in this study. We present hydrothermal pathways employed for the synthesis of NaTNT and HTNT in this study in Figure 1.

2.3. Characterization

Morphology of NaTNT and HTNT prepared was investigated using Transmission Electron Microscopy (TEM) which was operated at a voltage of 120 kV. X-ray diffraction (XRD) measurements of the prepared titanate derived materials were also performed. Furthermore, we equally used both Fourier Transform Infrared Spectroscopy (FTIR) and inductively coupled plasma atomic emission spectroscopy (ICP-AES) for the determination of functional groups and investigating elemental composition of both NaTNT and HTNT respectively to unravel the characteristic attributes responsible for the performance of the materials in our study. The characterization analyses are presented in the subsequent sections.

2.4. Photocatalytic degradation of MB

Degradation by the aid of the photocatalysis was investigated using Ultra-violet (UV) light on a 50 mL 10 $mg.L^{-1}$ MB solution (pH = 6.7) containing 0.5 $g.L^{-1}$ of the as-prepared catalysts for a duration between 30 min and 120 min. In the course of performing photocatalysis, we stirred the solution with the aid of as magnetic stirrer at room temperature (25 ± 2 °C). The mixture (MB/catalysts) was first made to undergo stirring under dark condition for duration of half hour in order to achieve homogenous distribution of MB molecules over the catalyst and *vice-versa* and subsequently applied the illumination of UV light. At 20 min range interval, 3 mL of the aliquot was taken and further centrifuged at 1000 revolution *per* min, for a duration of 5 min. A reactor box for the photocatalytic process of proportions 16 × 16 × 26 inches, with 8 W germicidal UV bulb (with energy > band gap of TiO_2 (3.2 eV)) as well as 78-1 magnetic stirrer hotplate was employed in this research (see Figure 2). The internal section of the box was painted black to reduce loss of light.

Thereafter, the concentration of the degraded MB solution (supernatant) was measured using 752W Ultra-violet (UV-Vis) Grating Spectrophotometer at a wavelength of maximum absorbance for MB (λ_{max} = 664 nm). The degradation efficiency of MB was measured using Eq. (1).

$$\text{Degradation } (\%) = \frac{Amount of MB degraded\ (C_t)}{Initial amount of MB\ (C_0)} \times 100 \qquad \text{Eqn. 1}$$

Where C_O is the initial dye concentration, C_t is the final dye concentration at the time, t. The rate constant (k) of degradation was evaluated using the pseudo-first order kinetic rate law [4, 8] as expressed in Eq. (2).

$$-In\frac{C_t}{C_0} = kt \qquad \text{Eqn. 2}$$

2.5. Reproducibility test

After photocatalytic each degradation test, the photocatalysts were collected using centrifuge. Subsequently, eluent agents (water and ethanol) were applied in the washing process. The photocatalysts recovered were oven dried at 100 °C for subsequent use in our next cycle of degradation activity.

2.6. Reactive oxygen species scavenging test

The reactive oxygen species (ROS) generated during photocatalytic reaction were experimentally determined by introducing 50 mM Na_2EDTA, 50 mM Cu $(NO_3)_2.3H_2O$, dimethyl sulphoxide (DMSO), and thiourea as scavengers for holes (h^+), electrons, and hydroxyl radical (OH) and superoxide radical ($O_2^{\bullet-}$), respectively.

3. Results and discussion

3.1. Characterisation of HTNT and NaTNT nanoparticles

According to the TEM analysis of our prepared photocatalysts shown in Figure 3, the P25 TiO_2 consists of nanoparticles (Figure 3a). Immediately the P25 TiO_2 sample was subjected to the treated with NaOH solution hydrothermal under specified parameters used for the preparation as mentioned earlier. Afterward, the resultant products obtained, NaTNT (Figure 3b) and was ion-exchanged using 0.1MHNO_3 solution

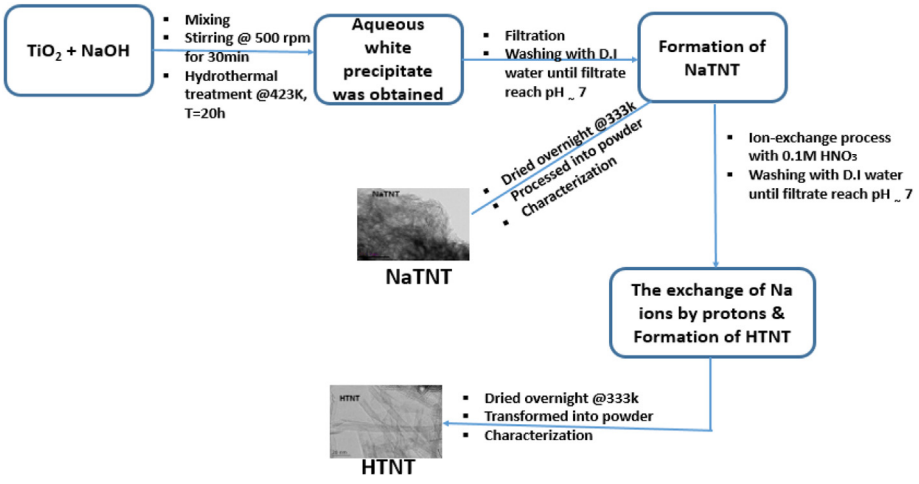

Figure 1. A schematic flow chart of hydrothermally obtained NaTNT and HTNT samples employed in this study.

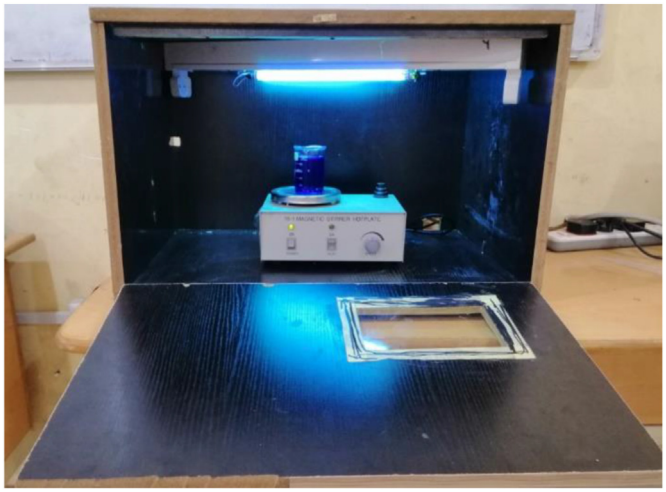

Figure 2. A black photolysis box with a magnetic stirrer and 8 W germicidal UV bulb.

thus HTNT produced (Figure 3c). According to the previously published report, the observed morphologies followed the path of a dissolution–reprecipitation mechanism [38]. The distinguished difference was due to the ion-exchange activities initiated during the synthesis of the materials. According to Figure 3d, the XRD patterns obtained revealed that the starting material P25 TiO_2 employed in the synthesis of NaTNT and HTNT majorly consists of anatase (JCPDS 84–1286) [47]. In another report, the NaTNT obtained exists as $NaHTi_2O_4(OH)_2$ phase (JCPDS 31–1329) [50]. According to the atomic ratio of sodium to titanium (Na/Ti) calculated using data obtained from ICP-AES report, ratio of NaTNT was found to be 0.34 (see Table 1). When NaTNT was ion-exchanged as earlier stated under preparation procedure, the peak at

Table 1. Estimated Na, Ti, and the Na/Ti atomic ratios of our prepared photocatalysts as determined by ICP-AES.

One dimensional (1D) Titanate materials	Na (Wt.%)	Ti (Wt.%)	Atomic ratio of Na/Ti
NaTNT	6.9	41.9	0.34
HTNT	0	48.0	0

10.2° previously saw got disappeared, furthermore the peak at 28.4° also diminished. We therefore attributed the phenomenon observed to the transition process from $NaHTi_2O_4(OH)_2$ phase (*i.e.* NaTNT) to $H_2Ti_2O_4(OH)_2$ phase (HTNT) (JCPDS 47–0124) [50]. To further confirm the transition of NaTNT to HTNT we equally use data obtained from ICP-AES to determine the sodium to titanium ratio (Na/Ti) and was found to be zero (0) (see Table 1) [47]. The sodium content in HTNT equal to zero was due to the total substitution of Na^+ ions with H^+ during the ion-exchange process. The difference in the Na/Ti atomic ratio of the prepared materials (HTNT&NaTNT)can be attributed to difference in preparation step and specifically ion-exchange process with HNO_3 solution causes the hydrogenation which led to the formation of HTNT as compared NaTNT, this type of hydrogenation through ion-exchange confirms a complete hydrogenation reaction [38, 50]. Moreover, the analysis of the XRD peaks revealed a reduction in the intensity ratio of Anatase/Rutile (I_A/I_R) from 2.00 in HTNT to 0.74 in the ion-exchange NaTNT, thus establishing the formation of rutile in the samples [4, 8]. The plausible routes used in this study for the preparation of titanate nanotubes (TNTs) are represented in Eqs. (3) and (4). As stated earlier NaTNT transformed to HTNT as a result of complete hydrogenation through ion-exchange step [47].

$$3TiO_2 + 2NaOH \rightarrow Na_2Ti_3O_7 + H_2O \quad \text{Eqn. 3}$$

$$Na_2Ti_3O_7 + 2H^+ \rightarrow 2Na^+ + H_2Ti_3O_7 \quad \text{Eqn. 4}$$

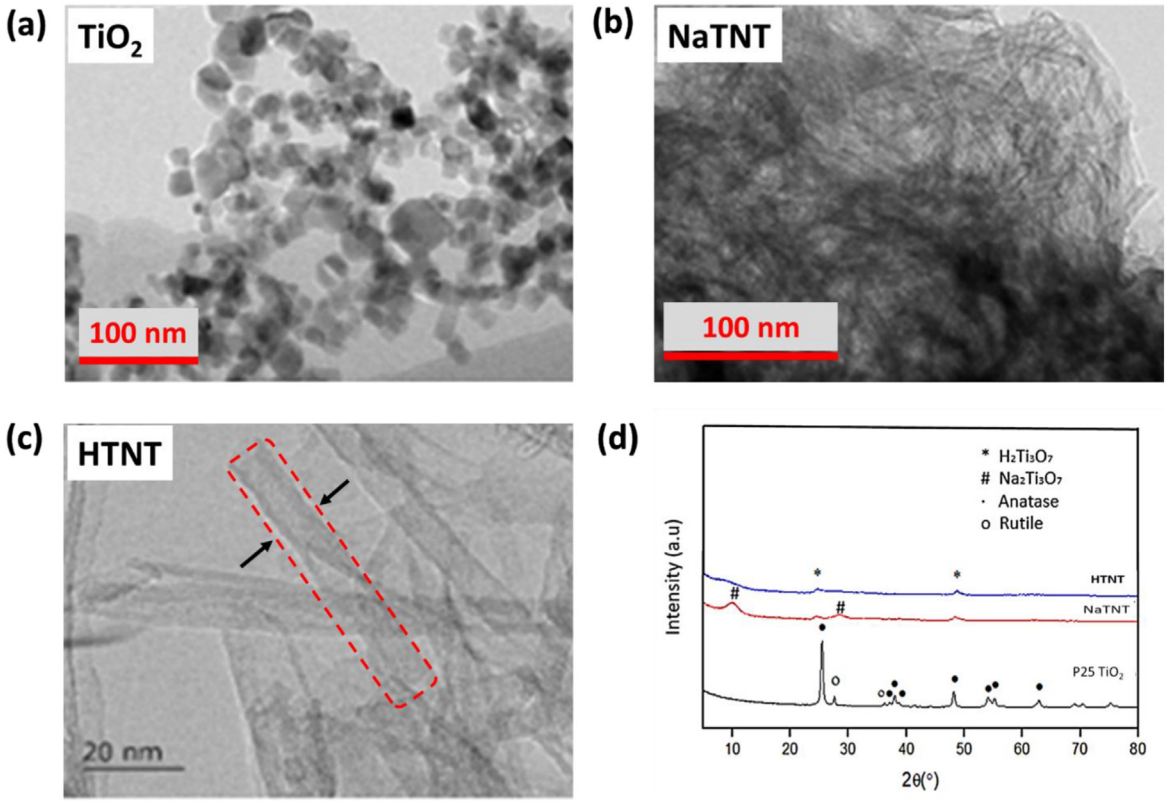

Figure 3. TEM images of (a) TiO_2 (b) NaTNT (c) HTNT; (d) XRD patterns of P25 TiO_2, NaTNT and HTNT.

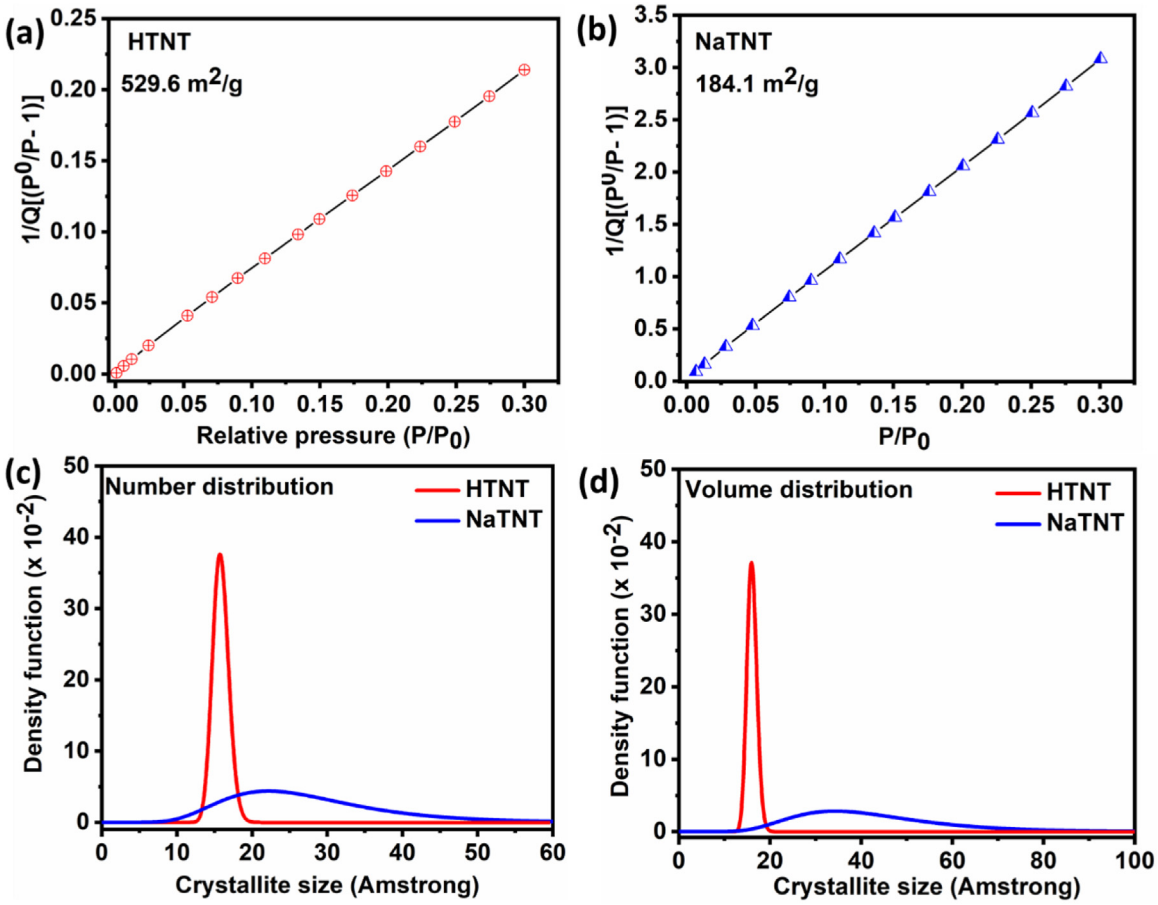

Figure 4. BET plot of (a) HTNT and (b) NaTNT; Particle size distribution in (c) number and (d) volume HTNT and NaTNT.

The surface area of HTNT and NaTNT was studied using the Brunauer-Emmett-Teller (BET) technique. From the analytical result obtained, the surface area of HTNT was far higher than NaTNT samples, as shown in Figure 4a and b, respectively. This may be attributed existence of Na atoms in the crystal matrix of TNTs, responsible for a particle size reduction observed in the photocatalyst. To confirm this intuition, particle size distribution analyses of these samples was performed. Figure 4c and dshow that the particle number and volume distribution of HTNT far exceeded those of NaTNT which are consistent with the BET results.

3.2. Photocatalytic degradation of methylene blue

3.2.1. Morphological effect on MB degradation by photocatalytic process

To monitor the efficiency of all the photocatalytic samples, degradation reaction was performed in the absence of photocatalyst (photolysis). In the photolysis test, the 10 mg.L^{-1} MB solution was irradiated at room temperature under constant stirring for 1.5 h. Figure 5a shows only a slight decrease in the conc. of MB. We investigated the photocatalytic degradation of 10 mg.L^{-1} MB at various contact times from 0.5 to 1.5 h using HTNT, NaTNT and P25 TiO_2as photocatalysts in the current study. Before illumination of UV light, the simulated pollutant solution containing the photocatalysts was stirred for just 30 min. in order to ensure equilibrium distribution of MB molecules on the surface of HTNT, NaTNT and P25 TiO_2. We observed interesting adsorption performance of the catalysts for MB in the dark phase (see Figure 5a). However, upon irradiation, the complete removal of MB was achieved. On the contrary, the case is totally different in the adsorption and photocatalytic degradation efficiency observed for P25 TiO_2which was comparatively low thus establishing the effect of morphology in the photocatalytic degradation of MB. Since HTNT and NaTNT displayed similar performance over the period of reaction, further kinetic study was carried to monitor their degradation over a relatively short-time interval as shown in Figure 5b. Overall, NaTNT showed better MB removal efficiency than HTNT as revealed in the insert in Figure 5b. The TNTs displayed higher degradation rates (Figure 5c). The rate constants of NaTNT and HTNT were calculated to be about 16 and 13 times that of P25 TiO_2. The lower performance of TiO_2 particles may be justified with high recombination of the photogenerated electron-hole (e^--h^+) pairs in the bulk of the nanoparticles [60]. On the contrary, the one-dimensional morphology of the as-prepared TNTs offers a facile vectorial movement of the photogenerated charge carriers, which implies lesser chances of recombination [61]. A maximum rate constant of 0.12 min^{-1} was observed in NaTNT. A significant contributing factor to the performance of the prepared samples is their high adsorption activity for MB. In the present study, the adsorption percentage of MB on the investigated photocatalysts was determined as presented in Figure 5d. The adsorption percentages of the as-prepared TNTs were both higher than P25 TiO_2, such performance was ascribed to higher surface area in HTNT and NaTNT. The surface area of HTNT is much larger than that of NaTNT, however, it is interesting to note a higher adsorption percentage in the latter. Such phenomenon may be ascribed to a stronger electrostatic interaction between the MB and the surface of the adsorbents, NaTNT [10].

3.2.2. Effect of photocatalyst dosage

Furthermore, the impact of the dosage of the as-prepared samples in the remediation of MB pollutant was investigated. The masses of HTNT and NaTNT were varied in the range 0.2–0.6 g/L under constant reaction conditions of 10 mg/L MB, 25 °C and stirring speed of 300 rpm. The increase in concentration of the prepared photocatalysts had no significant impact on the photocatalytic degradation of MB, as revealed in Figure 6a and b. In the case of HNT, the effect of dosage was only

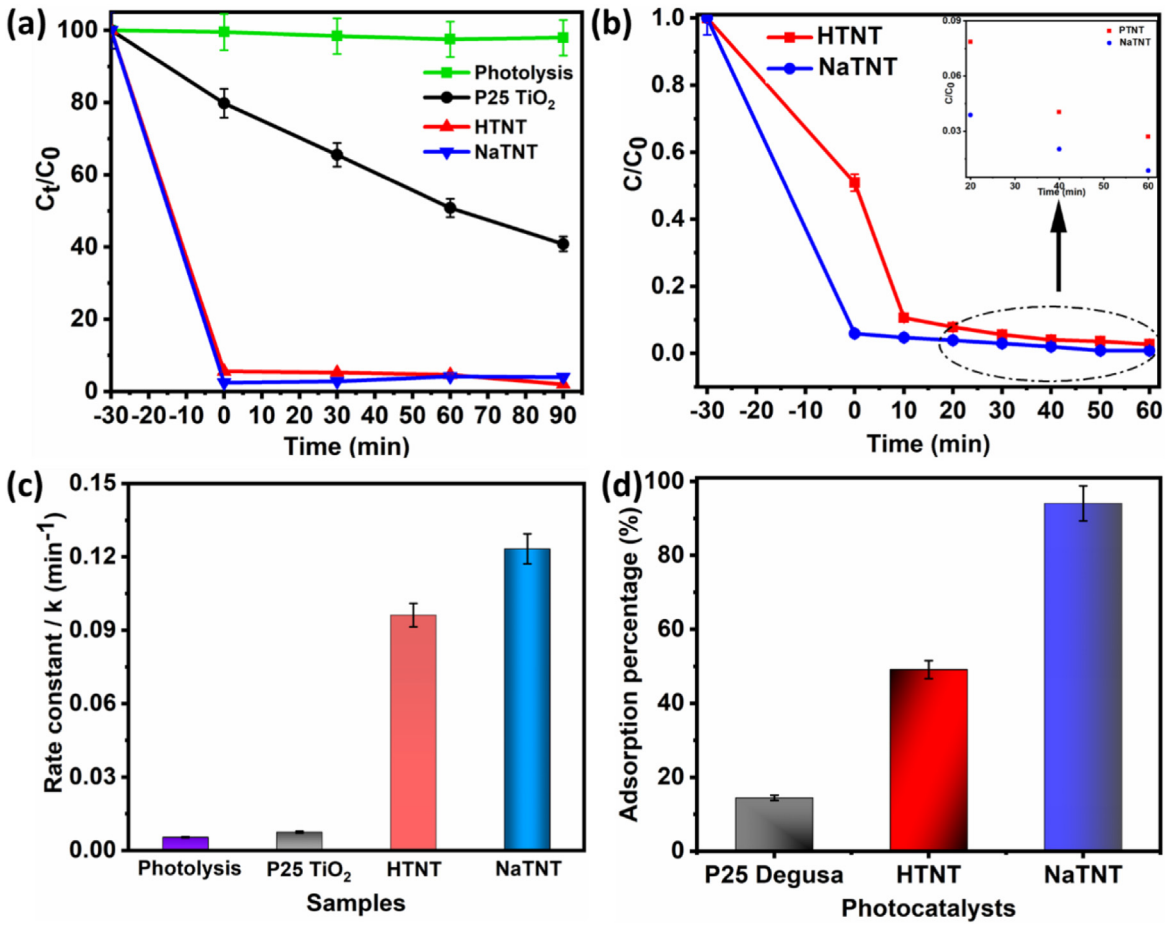

Figure 5. (a) Degradation of Methylene blue with photocatalysts (HTNT, NaTNT, and P25 TiO_2); (b) Degradation performance of HTNT and NaTNT (inset: showing difference); (c) Kinetic rate constants for photolysis and MB photocatalytic degradation using P25 TiO_2, HTNT and NaTNT (concentration of MB solution: 10 $mg.L^{-1}$; pH of MB solution = 6.7; reaction time: 1 h); (d) Adsorption percentage of P25 TiO_2, HTNT and NaTNT (mass of photocatalyst: 0.4 g/L; concentration of MB: 10 $mg.L^{-1}$; pH of MB solution = 6.7; reaction time: 1 h).

noticeable when 0.2 $g.L^{-1}$ was utilized particularly within the first 20 min of photocatalytic reaction. On the contrary, the removal rate of MB was changed by the amount of photocatalysts. Figure 6c shows an improved removal rate of MB with increase in the concentration of both HTNT and NaTNT. Overall, the NaTNT displayed a superior performance. The disparity in the effect of the charged masses in HTNT and NaTNT may be associated with electrostatic effect due to the presence of Na in the latter sample which enhances its performance.

3.2.3. *Effect of initial MB concentration*

The concentration of pollutants is one of the most crucial factors affecting their removal. The effect of the initial concentration of MB on the remediation efficiency of the as-prepared samples was investigated using different concentration of the pollutant in the range 1–30 $mg.L^{-1}$ and photodegradation reaction was performed under the same reaction condition as in previous experiments. Generally, the pollutant remediation performance of photocatalysts decreases with increase in the concentration of contaminants. Such was true in the case of HTNT as shown in Figure 7a, where the highest and lowest removal efficiency were observed in 10 $mg.L^{-1}$ and 30 $mg.L^{-1}$ MB, respectively. The as-prepared NaTNT displayed similar degradation performance under varying MB concentration (Figure 7b). However, the rate of degradation was observed to peak at 20 $mg.L^{-1}$ MB concentration, followed by a drastic decline at 30 $mg.L^{-1}$, as shown inset for Figure 7b. Related results on the influence of initial concentration of MB on its removal rate have been reported in the literatures [62, 63].

3.2.4. *Effect of pH*

Furthermore, using the as-prepared NaTNT photocatalyst as a model, the influence of pH on the degradation of MB via photocatalysis in the pH range from 2.0 to12.0was also studied. In the process of doing this we adjusted the pH of the MB with 0.1 M HCl and 0.1 M NaOH solutions. In the dark phase reaction (adsorption), at pH 6, NaTNT demonstrated highest adsorption performance while at pH 2.0 and 12.0, as shown in Figure 8a lower rates were noticed respectively. The observed lower degradation performance of the photocatalyst at these areas is associated with the high concentration of the competing ions (H^+ and OH^-). The point of zero charge (PZC) of the adsorbent was determined to further explore the adsorption mechanism. The PZC experiment was performed by agitating a suspension of 20 mg NaTNT in a predetermined pH of 0.1 M $NaNO_3$ overnight in an orbital shaker at room temperature and the final pH of the supernatant was recorded after shaking. The PZC plot in Figure 8b reveals the PZC of NaTNT adsorbents to be 2.06. At this pH the sample displays a net charge of zero. In the present study, at pH 2.0 (pH < PZC), the NaTNT was positively charge and a decrease in adsorption of cationic MB was observed due to electrostatic repulsion. At a pH 6.0 (pH > PZC), the surface of the adsorbents was negatively charge and its absorption for cationic MB was enhanced because of electrostatic attraction. In addition, increase in pH led to a reduction in the adsorption of MB, which may be ascribed to the high stability of MB under alkaline medium [64, 65]. Interestingly, a degradation performance more than 99% was attained within 10 min of light illumination under pH 12.0. One plausible explanation for this phenomenon is the presence of Na^+ ions

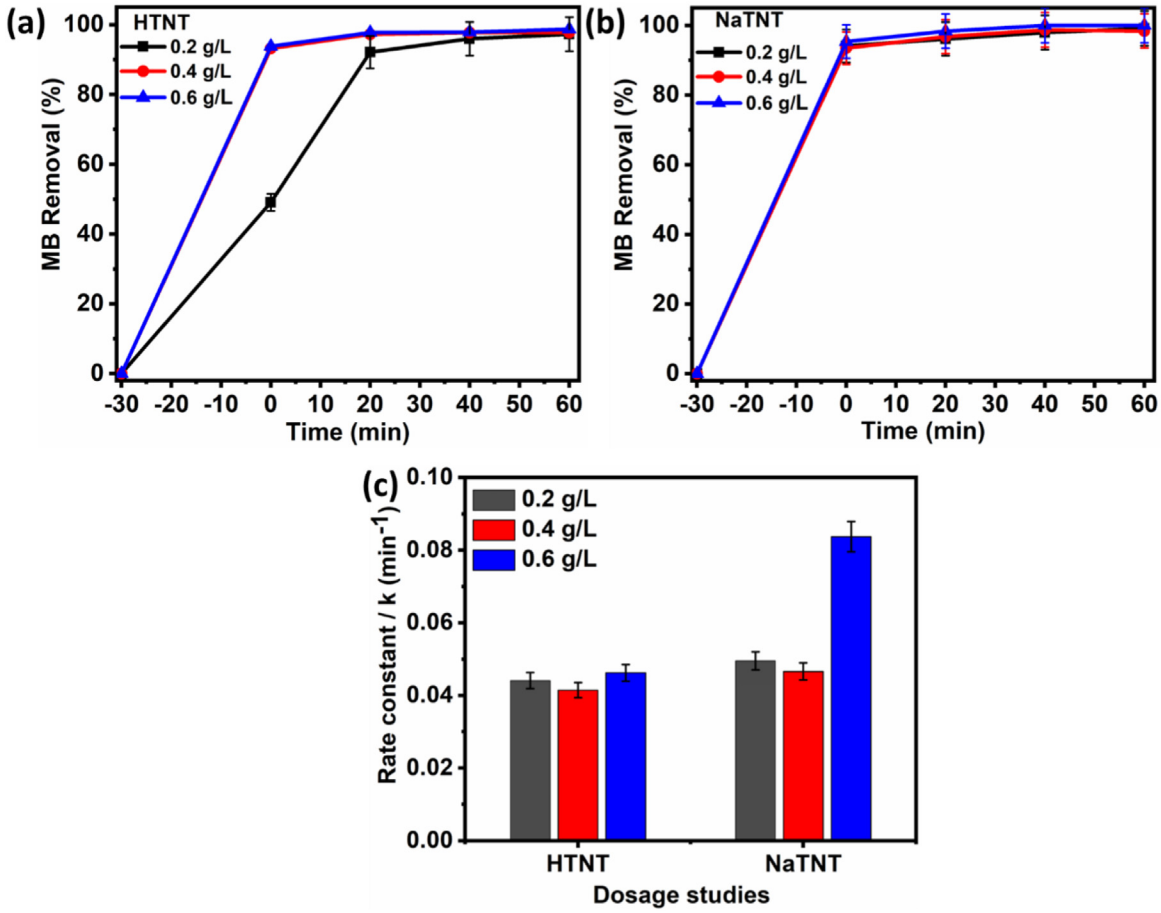

Figure 6. Effect of dosage on the photocatalytic degradation of MB using (a) HTNT and (b) NaTNT; (c) dosage effect on the rate constants of HTNT and NaTNT (dosage of photocatalyst: 0.2–0.6 g/L; concentration of MB solution: 10 mg.L^{-1}; pH of MB solution = 6.7; reaction time:1 h).

introduced during pH adjustment using NaOH. These ions capture the photogenerated electrons during photocatalysis, thereby reducing charge carrier recombination giving rise to enhanced degradation of MB. On the contrary, the degradation performance of the NaTNT photocatalyst was relatively poor under pH 2.0 since H^+ ions present in reaction solution are not suitable minimizing for charge carrier recombination. To investigate change in the pH of the MB solution during degradation, a separate reaction was performed under neutral medium of MB (pH 6.7) and the final pH after degradation reaction was measured to be 8.48.

3.2.5. *Reusability and stability*

The reusability of the as-prepared NaTNT photocatalyst was examined through repeated runs of photocatalytic degradation of 10 mg/L MB. It was observed that the performance of the sample was relatively constant after five cycles as shown in Figure 9a. The good reproducibility of the as-prepared NaTNT photocatalyst suggests its potential applicability in large scale wastewater treatment barring other parameters. Furthermore, FTIR peaks ofthe NaTNT before and after photocatalytic reaction shows good stability of the samples (Figure 9b). Besides, the

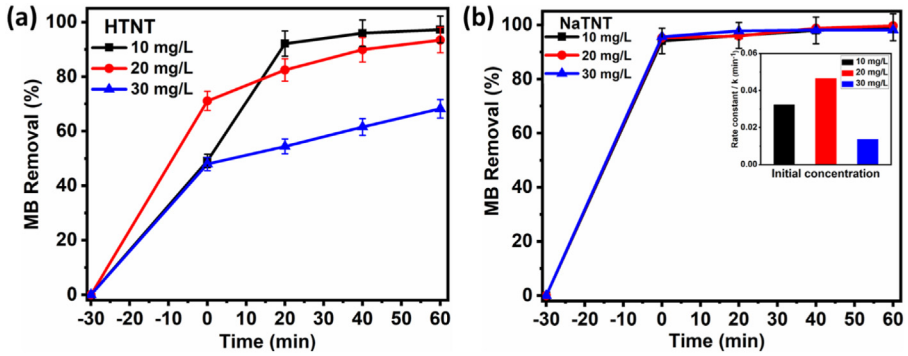

Figure 7. Effect of initial concentration of MB on the photocatalytic degradation of MB using (a) HTNT and (b) NaTNT; available inset, is the photocatalytic degradation of MB under varying initial concentration of MB (mass of photocatalyst: 0.4 g.L^{-1}; initial concentration of MB: 10–30 mg.L^{-1}; pH of MB solution = 6.7; reaction time:1 h).

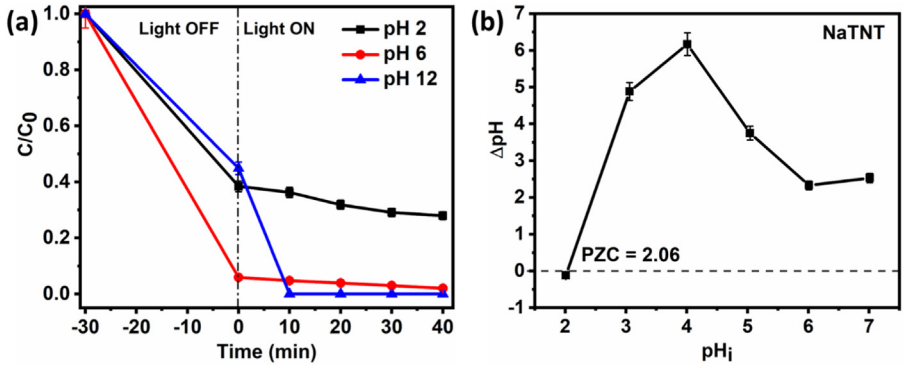

Figure 8. (a) Effect of pH on photodegradation performance of NaTNT; (b) Point of zero charge of NaTNT (mass of photocatalyst: 0.4 $g.L^{-1}$; concentration of MB: 10 $mg.L^{-1}$; reaction time: 40 min).

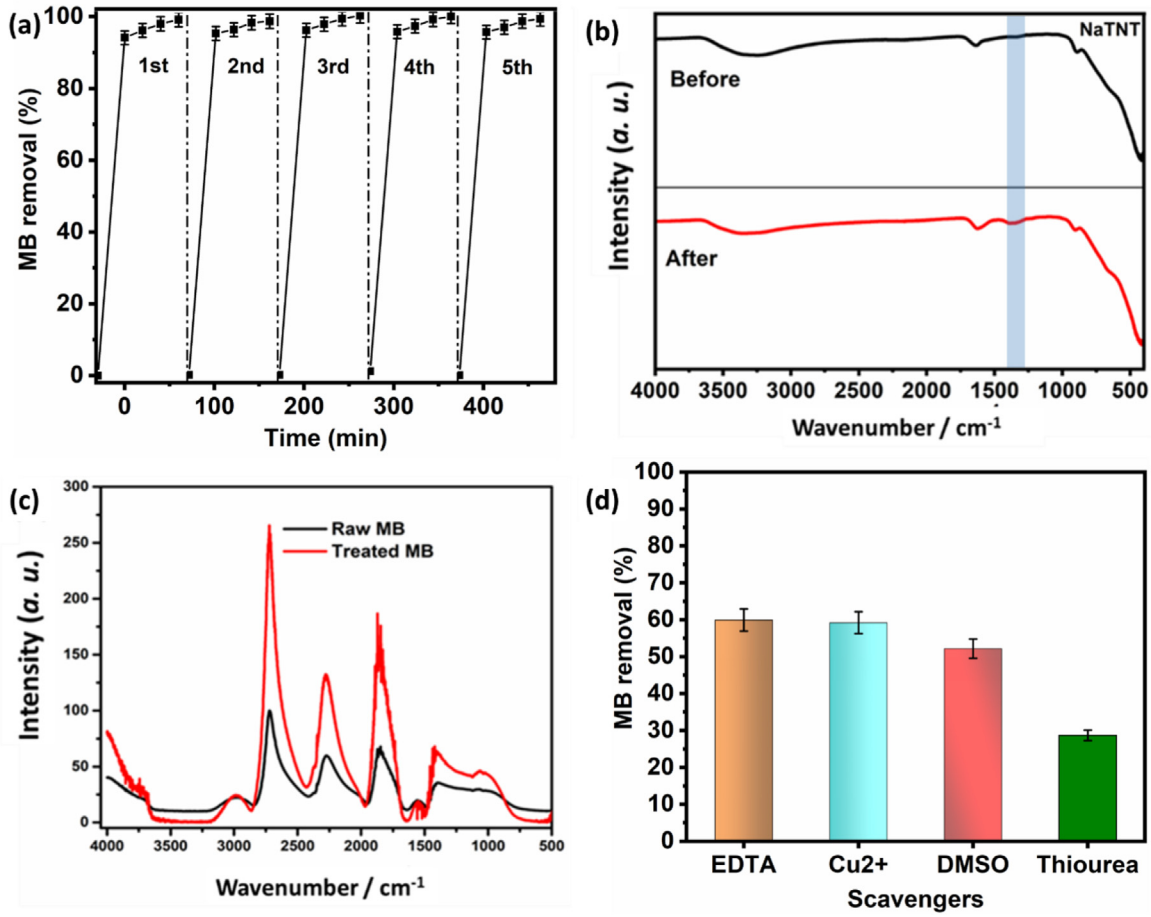

Figure 9. (a) Reusability test of as-prepared NaTNT; (b) FTIR spectra of raw and used NaTNT; (c) raw and treated MB; (d) experimental determination of reactive species in the degradation of MB (mass of photocatalyst: 0.4 $g.L^{-1}$; concentration of MB: 10 $mg.L^{-1}$; reaction time: 40 min) by photocatalysis.

Table 2. Comparison of MB removal efficiencies of various adsorbents with titanate derived adsorbents employed in this work under light irradiation.

Various Adsorbents/Amount	Preparation Method	Dye Conc. (mg/L)	Light Source	Degradation rate of MB (%) *per* Time	Ref
RGO/TiO_2 nanocomposites (0.5 g/L)	Chemical exfoliation	6.4	UV-light	86% at 60 min	[66]
RGO/TiO_2 nanocomposites (0.5 g/L)	Chemical exfoliation	6.4	Visible light	81% at 60 min	[66]
Zr_3O/AC. (0.2 g/L)	Chemical Impregnation/pyrolysis	80	UV-light	84.81% at 120min	[67]
-Fe_3/Fe_3O_4/SiO_2 (Ar modified)	Single stage heat-treatment process	50	UV-light	87.5% at 120 min	[68]
CuO/Bi_2O_3 Nanocomposite (0.2 g/L)	Impregnation calcination method	50	UV-C irradiation	88.32% at 120 min	[69]
Na-TNTs (0.5 g/L)	Hydrothermal method	10	8 W germicidal UV bulb	98.5% at 60 min	This work
H-TNTs (0.5 g/L)	Hydrothermal method	10	8 W germicidal UV bulb	95.10 % at 60 min	This work

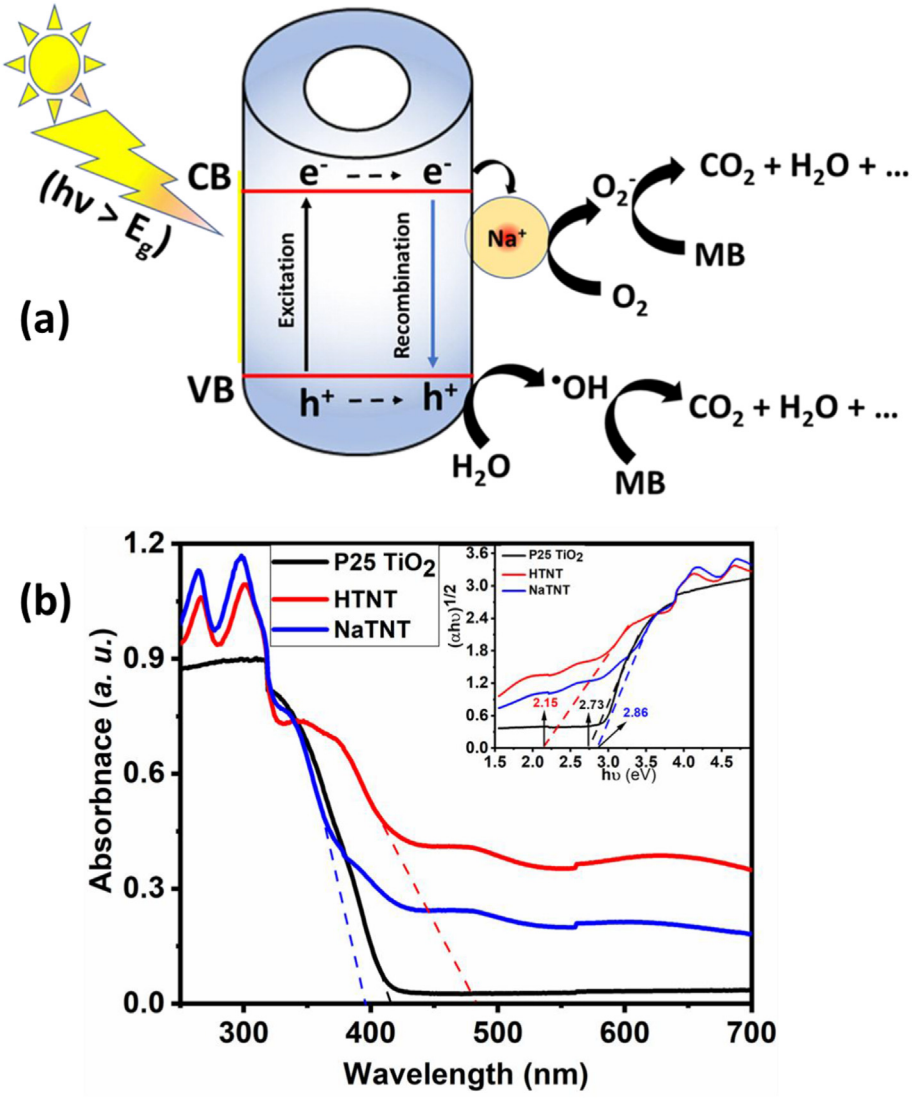

Figure 10. (a) The mechanism for photocatalytic degradation of MB molecules using NaTNT; (b) UV-Vis DRS of P25 TiO_2, HTNT, and NaTNT (Inset: band gap plot of photocatalysts).

change in the functional groups of NaTNT due to interaction with the pollutant was also investigated. At adopted reaction temperature for the hydrothermal reaction, we propose a plausible pathway for the breaking of the Ti–O–Ti bond and the replacement of the broken bond with Na^+ and –OH for the formation of a new bond with Ti–O–Na and Ti–OH bonds [53], at synthesis stage and were affirmed in the raw NaTNT. The wide peaks observed at 3297∼3400 cm^{-1} are assigned to the broadening vibration of the O–H which confirms the adsorption of water molecules on the surface of the catalyst while the observed peak at 1755 cm^{-1} is attributed to availability and presence of H–O–H in the non-treated sample which shifted to 1800cm^{-1} in the treated TNTs [29]. The bands around 547 $cm^{-1}$are ascribed to the presence of both Ti–O and Ti–O–Ti in the region [29, 53]. A comparative FTIR analysis was performed to ascertain the peak differences between the fresh and used NaTNT. A new peak can be observed around 1412 cm^{-1}, which may be associated with the interaction between MB and NaTNT.

On the other hand, the change in the FTIR spectra of raw and treated MBwas investigated to ascertain the likely participation of the functional groups inthe adsorption process (Figure 9c). For the rawMB, a peak appears at 2844 cm^{-1} which shifted to 2864 cm^{-1}in the treated sample, represents the stretching vibration of –CH– aromatic, while 1454 cm^{-1} represents $–CH_3$ groups. The bands from 1541 to 1401 cm^{-1} are ascribed to the existence of aromatic ring structures. The spectra 3598 and 3142 cm^{-1} signify –OH and N–H aromatic amine correspondingly. The peak at 1632 cm^{-1} stands for –C=O, while the peak ranging from 1694 cm^{-1} is linked to the availability of C=C present in the aromatic rings. The observed peaks 1875 cm^{-1}, 2225 cm^{-1}, and 2864 $cm^{-1}$of the MB sample (red line) indicate its adsorption on the prepared NaTNT. Table 2 shows the comparison of this work with previously published reports on the degradation of MB using various photocatalysts.

3.3. Photodegradation mechanism

The reactive oxygen species (ROS) responsible for the photocatalytic degradation of MB were experimentally determined by introducing salts of Na_2EDTA, $Cu(NO_3)_2.3H_2O$, dimethyl sulphoxide (DMSO), and thiourea as scavengers for holes (h^+), electrons, hydroxyl radical (OH^-) and superoxide radical (O_2^{*-}), respectively. Comparatively, a significant decrease in the degradation of MB was observed in the presence of thiourea, thus suggesting O_2^{*-} as the dominant ROS in the photocatalysis (Figure 9d). Closely followed by it is the •OH, as evidenced by the slight decrease in the degradation of MB as DMSO was introduced. A plausible mechanism for the degradation of MB via photocatalysis using NaTNT illustrated in Figure 10a. The photogenerated charges are formed according to Eq. (5) upon illumination with UV light.

$$NaTNT + hv \rightarrow e_{CB}^{-} + h_{VB}^{+} \quad \text{Eqn. 5}$$

The photogenerated electrons migrate to the conduction band (CB) and take part in the following reactions (Eqs. (6) and (7)). The presence of ion-exchanged sodium ions on the NaTNT (evidenced from the ICP-AES) further generates more of the dominant ROS (O_2^{*-}) by attracting the photogenerated electrons (Eqn. 6). The O_2^{*-} reacts with water molecules to generate •OH (Eqn. 7), which has the potential to degrade MB into smaller molecules (Eqn. 8).

$$e_{CB}^{-} + O_2 \rightarrow O_2^{*-} \text{ (superoxide radicals)} \quad \text{Eqn. 6}$$

$$H_2O + O_2^{*-} \rightarrow HO_2^{*} \text{(hydroperoxy radical)} + \cdot OH \quad \text{Eqn. 7}$$

$$\bullet OH + MB \rightarrow Intermediates \rightarrow H_2O + CO_2 \quad \text{Eqn. 8}$$

On the other hand, the photogenerated holes in the valence band (VB) move to the surface of the NaTNT, reacts with water molecules and leads to the formation of •OH (Eqn. 9), which are utilized in the degradation of MB.

$$h_{VB}^{+} + H_2O \rightarrow \bullet OH \quad \text{Eqn. 9}$$

The light absorption activities and bandgaps (E_g) of the samples was investigated using UV-Vis diffuse reflectance spectroscopy (DRS) and the Tauc plot to further unravel the rationale for their varying performance. Figure 10b shows the visible light absorbance and Tauc plot (insert) of P25 TiO_2, HTNT, and NaTNT.The HTNT demonstrated an enhanced visible light absorption (482 nm) relative to P25 TiO_{2v} (415 nm), while NaTNT displayed a blue shift (394 nm). Correspondingly, the E_g of P25 TiO_2, HTNT, and NaTNT were calculated to be 2.73 eV, 2.15 eV and 2.86 eV respectively. Therefore, the superior performance of the NaTNT may be associated to its higher activity in the irradiated UV light (evidenced from its blue shift and larger E_g). Based on these, the performance of NaTNT could be attributed to the cation exchange mechanistic activities that took place during acid washing (see Eqs. (3) and (4)) which was previously accounted for in the adsorption of cationic dyes on TNTs [70, 71, 72, 73, 74].

4. Conclusion

Complementary ion-exchange HTNT and NaTNT were synthesised by hydrothermal method. Photodegradation studies reveal an enhanced performance using the as-prepared TNTs in comparison to commercial P25 TiO_2. Adsorption capacity of the ion-exchange TNTs was experimented to play a significant role in the photodegradation of MB. The ion-exchange NaTNT showed better a performance than HNT samples. The enhanced adsorption and photocatalytic performance of NaTNT was associated to its electrostatic interaction with MB and higher photoactivity in UV light (due to larger band gap). The photocatalytic degradation performance was investigated to be associated with reactive oxygen species and O_2^{*-} was observed to be a key component. Additionally, after five cycles of experiment, the ion-exchange NaTNT demonstrated a good reusability and stability as evidenced by the FTIR results.

The limitation of this research is hinged on the fact that hydrothermal technique requires the use of expensive autoclave, high power consumption, long reaction time, safety issue(s) during reaction period and the inability to monitor reaction conditions.

Declarations

Author contribution statement

Aderemi Timothy Adeleye, Kingsley Igenepo John: Conceived and designed the experiments; Performed the experiments; Analyzed and interpreted the data; Wrote the paper.

Joshua O. Ighalo: Conceived and designed the experiments; Analyzed and interpreted the data.

Samuel Ogunniyi, Comfort Abidemi Adeyanju, Martins O. Omorogie: Analyzed and interpreted the data; Wrote the paper.

Mohammed Elawad: Analyzed and interpreted the data.

Adewale George Adeniyi: Conceived and designed the experiments; Analyzed and interpreted the data; Contributed reagents, materials, analysis tools or data.

Funding statement

This research did not receive any specific grant from funding agencies in the public, commercial, or not-for-profit sectors.

Data availability statement

Data will be made available on request.

Declaration of interest's statement

The authors declare no conflict of interest.

Additional information

No additional information is available for this paper.

Acknowledgements

All Authors whose works were cited are hereby acknowledged.

References

[1] I. Tantis, et al., Coupling of electrochemical and photocatalytic technologies for accelerating degradation of organic pollutants, J. Photochem. Photobiol. Chem. 317 (2016) 100–107.
[2] P. Papazotos, Potentially toxic elements in groundwater: a hotspot research topic in environmental science and pollution research, Environ. Sci. Pollut. Res. Int. 28 (35) (2021) 47825–47837.
[3] J.O. Adeyemi, T. Ajiboye, D.C. Onwudiwe, Mineralization of antibiotics in wastewater via photocatalysis, Water Air Soil Pollut. 232 (5) (2021).
[4] K.I. John, et al., Oxygen deficiency induction and boundary layer modulation for improved adsorption performance of titania nanoparticles, Chem. Pap. 76 (6) (2022) 3829–3840.
[5] Kingsley I. John, M.O. Omorogie, Ajibola A. Bayode, T. Aderemi, Adeleye, Brigitte Helmreich, Environmental microplastics and their additives—a critical review on advanced oxidative techniques for their removal, Chem. Pap. (2022).
[6] T.F. Guerin, Using prototyping to minimise remediation costs: a case study on a former paint factory, Water Air Soil Pollut. 232 (6) (2021).
[7] E. Issaka, et al., Biochar-based composites for remediation of polluted wastewater and soil environments: challenges and prospects, Chemosphere 297 (2022) 134163.
[8] K. Igenepo John, et al., Unravelling the effect of crystal dislocation density and microstrain of titanium dioxide nanoparticles on tetracycline removal performance, Chem. Phys. Lett. 776 (2021) 138725.
[9] D. Balarak, et al., Adsorption of acid blue 92 dye from aqueous solutions by single-walled carbon nanotubes: isothermal, kinetic, and thermodynamic studies, Environ. Proc. 8 (2) (2021) 869–888.
[10] S. Karthi, et al., Removal of methylene blue dye using shrimp shell chitin from industrial effluents, Mater. Today Proc. 66 (4) (2022) 1945–1950.
[11] T.P.K. Kulasooriya, N. Priyantha, A.N. Navaratne, Removal of textile dyes from industrial effluents using burnt brick pieces: adsorption isotherms, kinetics and desorption, SN Appl. Sci. 2 (11) (2020).
[12] L. Hevira, et al., Terminalia catappa shell as low-cost biosorbent for the removal of methylene blue from aqueous solutions, J. Ind. Eng. Chem. 97 (2021) 188–199.
[13] N. Mehmandost, et al., Removal of methylene blue and crystal violet in binary aqueous solution by magnetic Terminalia catappa kernel shell biosorbent using Box–Behnken design, J. Iran. Chem. Soc. 19 (9) (2022) 3769–3781.
[14] K.I. John, et al., Effect of light on concomitant sequestration of Cu(II) and photodegradation of tetracycline by H-MOR/H-β/H-ZSM-5 zeolites, Environ. Sci. Pollut. Res. Int. 29 (8) (2021) 11756–11764.
[15] J. Su, et al., Efficient arsenic removal by a bifunctional heterogeneous catalyst through simultaneous hydrogen peroxide (H_2O_2) catalytic oxidation and adsorption, J. Clean. Prod. 325 (2021) 129329.
[16] O.S. Awofiranye, S.J. Modise, E.B. Naidoo, Overview of polymer–TiO_2 catalyst for aqueous degradation of pharmaceuticals in heterogeneous photocatalytic process, J. Nanoparticle Res. Interdis. For. Nanosc. Sci. Techn. 22 (6) (2020).

[17] E. Brillas, A review on the photoelectro-Fenton process as efficient electrochemical advanced oxidation for wastewater remediation. Treatment with UV light, sunlight, and coupling with conventional and other photo-assisted advanced technologies, Chemosphere 250 (2020) 126198.

[18] C.M. Martinez, et al., Ozonation for remediation of pesticide-contaminated soils at field scale, Chem. Eng. J. 446 (2022) 137182. Lausanne, Switzerland: 1996.

[19] S. Gita, et al., Adsorption–biodegradation coupled remediation process for the efficient removal of a textile dye through chemically functionalized sugarcane bagasse, Water Environ. Res. 93 (10) (2021) 2223–2236.

[20] Y. Xiang, J. Fang, C. Shang, Kinetics and pathways of ibuprofen degradation by the UV/chlorine advanced oxidation process, Water Res. 90 (2016) 301–308.

[21] S. Sousa, et al., Organochlorine pesticides removal from wastewater by pine bark adsorption after activated sludge treatment, Environ. Technol. 32 (6) (2011) 673–683.

[22] Y. Cherni, et al., Detoxification of leachate by coagulation treatment prior to fermentation and possible reuse in irrigation, Clean: Soil, Air, Water 50 (6) (2022) 2000395.

[23] F. Hassan, et al., Fabrication of graphene-oxide and zeolite loaded polyvinylidene fluoride reverse osmosis membrane for saltwater remediation, Chemosphere 307 (2022) 136012.

[24] T. Kousar, et al., SnO_2/UV/H_2O_2 and TiO_2/UV/H_2O_2 efficiency for the degradation of reactive yellow 160A: by-product distribution, cytotoxicity and mutagenicity evaluation, Catalysts 12 (5) (2022) 553.

[25] J. Singh, A.K. Manna, R.K. Soni, Bifunctional Au–TiO_2 thin films with enhanced photocatalytic activity and SERS based multiplexed detection of organic pollutant, J. Mater. Sci. Mater. Electron. 30 (17) (2019) 16478–16493.

[26] D. Nunes, et al., Metal oxide-based photocatalytic paper: a green alternative for environmental remediation, Catalysts 11 (4) (2021) 504.

[27] A. Vahl, et al., Pathways to tailor photocatalytic performance of TiO_2 thin films deposited by reactive magnetron sputtering, Materials 12 (17) (2019) 2840.

[28] G. Zhang, et al., Electrospinning directly synthesized metal nanoparticles decorated on both sidewalls of TiO_2 nanotubes and their application, Electronic supplementary information (ESI) 5 (13) (2013) 581–588.

[29] A. Maira, et al., Fourier transform infrared study of the performance of nanostructured TiO_2 particles for the photocatalytic oxidation of gaseous toluene, J. Catal. 202 (2) (2001) 413–420.

[30] K.-L. Chan, et al., Photocatalytic performance of bipyramidal anatase TiO_2 toward the degradation organic dyes and its catalyst poisoning effect, React. Kinet. Mech. Catal. 130 (1) (2020) 531–546.

[31] M. Abdullah, S.K. Kamarudin, Titanium dioxide nanotubes (TNT) in energy and environmental applications: an overview, Renew. Sustain. Energy Rev. 76 (2017) 212–225.

[32] K. Ahmad, et al., Influence of electrochemical reduction on the optical properties of TiO_2 nanotubes under ambient conditions, Appl. Phys. Mater. Sci. Process 127 (8) (2021).

[33] S. Mathew, et al., Metal-Doped titanium dioxide for environmental remediation, hydrogen evolution and sensing: a review, ChemistrySelect 6 (45) (2021) 12742–12751.

[34] H.-Y. Wu, et al., Photocatalytic reduction of CO_2 using molybdenum-doped titanate nanotubes in a MEA solution, RSC Adv. 5 (78) (2015) 63142–63151.

[35] D. Dolat, et al., Nitrogen-doped, metal-modified rutile titanium dioxide as photocatalysts for water remediation, Appl. Catal. B Environ. 162 (2015) 310–318.

[36] H. Sun, et al., Visible light responsive titania photocatalysts codoped by nitrogen and metal (Fe, Ni, Ag, or Pt) for remediation of aqueous pollutants, Chem. Eng. J. 231 (2013) 18–25. Lausanne, Switzerland: 1996.

[37] C. Lim, et al., Carbon-titanium dioxide heterogeneous (photo)catalysts (C–TiO_2) for highly efficient visible light photocatalytic application, Compos. B Eng. 241 (2022) 109997.

[38] M.N. Subramaniam, et al., Adsorption and photocatalytic degradation of methylene blue using high surface area titanate nanotubes (TNT) synthesized via hydrothermal method, J. Nanoparticle Res. : Interdis. For. Nanosc. Sci. Techn. 19 (6) (2017) 220.

[39] T. Tan, D. Beydoun, R. Amal, Effects of organic hole scavengers on the photocatalytic reduction of selenium anions, J. Photochem. Photobiol. Chem. 159 (3) (2003) 273–280.

[40] S. Khayyat, L. Selva Roselin, Photocatalytic degradation of benzothiophene and dibenzothiophene using supported gold nanoparticle, J. Saudi Chem. Soc. 21 (3) (2017) 349–357.

[41] M. Al-Mamun, et al., Photocatalytic activity improvement and application of UV-TiO_2 photocatalysis in textile wastewater treatment: a review, J. Environ. Chem. Eng. 7 (5) (2019) 103248.

[42] M. Kocijan, et al., Graphene-based TiO_2 nanocomposite for photocatalytic degradation of dyes in aqueous solution under solar-like radiation, Appl. Sci. 11 (9) (2021) 3966.

[43] M. Kocijan, et al., Immobilised rGO/TiO_2 nanocomposite for multi-cycle removal of methylene blue dye from an aqueous medium, Appl. Sci. 12 (1) (2021) 385.

[44] A.S. Ganie, et al., Nanoremediation technologies for sustainable remediation of contaminated environments: recent advances and challenges, Chemosphere 275 (2021) 130065.

[45] M. Sun, et al., Synthesis of Cu_2O/graphene/rutile TiO_2 nanorod ternary composites with enhanced photocatalytic activity, J. Alloys Compd. 650 (2015) 520–527.

[46] A.T. Adeleye, et al., One-dimensional titanate nanotube materials: heterogeneous solid catalysts for sustainable synthesis of biofuel precursors/value-added chemicals—a review, J. Mater. Sci. 56 (33) (2021) 18391–18416.

[47] A.A. Timothy, et al., Synthesis of jet fuel range high-density dicycloalkanes with methyl benzaldehyde and acetone, Sustain. Energy Fuels 4 (11) (2020) 5560–5567.

[48] S. Ghafoor, et al., TiO_2 nanofibers embedded with g-C_3N_4 nanosheets and decorated with Ag nanoparticles as Z-scheme photocatalysts for environmental remediation, J. Environ. Chem. Eng. 7 (6) (2019) 103452.

[49] M.G.A. Saleh, A.A. Badawy, A.F. Ghanem, Using of titanate nanowires in removal of lead ions from waste water and its biological activity, Inorg. Chem. Commun. 108 (2019) 107508.

[50] T. Kasuga, et al., Titania nanotubes prepared by chemical processing, Adv. Mater. 11 (15) (1999) 1307–1311.

[51] N.A.M. Barakat, et al., FexCo1−x-doped titanium oxide nanotubes as effective photocatalysts for hydrogen extraction from ammonium phosphate, Int. J. Hydrogen Energy 43 (16) (2018) 7990–7997.

[52] M.S. Mahmoud, et al., Influence of Mn, Cu, and Cd–doping for titanium oxide nanotubes on the photocatalytic activity toward water splitting under visible light irradiation, Colloids Surf. A Physicochem. Eng. Asp. 554 (2018) 100–109.

[53] S. Muniyappan, et al., Conventional hydrothermal synthesis of titanate nanotubes: systematic discussions on structural, optical, thermal and morphological properties, Mod. Electr. Mater. 3 (4) (2017) 174–178.

[54] U.H. Shah, et al., Investigation of the formation mechanism of titanium oxide nanotubes and its electrochemical evaluation, J. Appl. Electrochem. 47 (10) (2017) 1147–1159.

[55] O.I. Kalu, et al., A novel approach to the sol–gel synthesis of titanium dioxide-coated SBA-16 type silica mesoporous microspheres for water purification, Materialia 5 (2019) 100237.

[56] H. Wang, et al., Template synthesis and characterization of TiO_2 nanotube arrays by the electrodeposition method, Mater. Lett. 93 (2013) 319–321.

[57] P. Nakpan, A. Aeimbhu, Fabrication of titanium dioxide nanotubes by difference the anodization voltage and time, Mater. Today Proc. 47 (2021) 3436–3440.

[58] M. Sluban, et al., Protonated titanate nanotubes as solid acid catalyst for aldol condensation, J. Catal. 346 (2017) 161–169.

[59] M. Kitano, et al., Protonated titanate nanotubes as solid acid catalyst, J. Am. Chem. Soc. 132 (19) (2010) 6622–6623.

[60] K. Ozawa, et al., Electron–hole recombination time at TiO_2 single-crystal surfaces: influence of surface band bending, J. Phys. Chem. Lett. 5 (11) (2014) 1953–1957.

[61] A. Aronne, et al., Electronic properties of TiO_2 -based materials characterized by high Ti^{3+} self-doping and low recombination rate of electron–hole pairs, RSC Adv. 7 (4) (2017) 2373–2381.

[62] V.L.E. Siong, et al., Removal of methylene blue dye by solvothermally reduced graphene oxide: a metal-free adsorption and photodegradation method, RSC Adv. 9 (64) (2019) 37686–37695.

[63] S. Alkaykh, A. Mbarek, E.E. Ali-Shattle, Photocatalytic degradation of methylene blue dye in aqueous solution by $MnTiO_3$ nanoparticles under sunlight irradiation, Heliyon 6 (4) (2020), e03663.

[64] Y. Zhang, et al., Adsorption of methylene blue from aqueous solution using gelatin-based carboxylic acid-functionalized carbon Nanotubes@Metal–organic framework composite beads, Nanomaterials 12 (15) (2022) 2533.

[65] X. Zou, et al., Preparation and characterization of polyacrylamide/sodium alginate microspheres and its adsorption of MB dye, Colloids Surf. A Physicochem. Eng. Asp. 567 (2019) 184–192.

[66] M.A.E. Wafi, et al., Exceptional removal of methylene blue and p-aminophenol dye over novel TiO_2/RGO nanocomposites by tandem adsorption-photocatalytic processes, Mater. Sci. Energy Techn. 5 (2022) 217–231.

[67] H. Ait Ahsaine, et al., Adsorptive removal of methylene blue and crystal violet onto micro-mesoporous Zr_3O/activated carbon composite: a joint experimental and statistical modeling considerations, J. Chem. 2018 (2018).

[68] M.M.S. Sanad, et al., Preparation and characterization of magnetic photocatalyst from the banded iron formation for effective photodegradation of methylene blue under UV and visible illumination, J. Environ. Chem. Eng. 9 (2) (2021) 105127.

[69] F. Poorsajadi, et al., Synthesis of CuO/Bi_2O_3 nanocomposite for efficient and recycling photodegradation of methylene blue dye, Int. J. Environ. Anal. Chem. (2020) 1–14.

[70] C.-K. Lee, et al., Effects of synthesis temperature on the microstructures and basic dyes adsorption of titanate nanotubes, J. Hazard Mater. 150 (3) (2008) 494–503.

[71] C.-K. Lee, et al., Effects of sodium content on the microstructures and basic dye cation exchange of titanate nanotubes, Colloids Surf. A Physicochem. Eng. Asp. 317 (1-3) (2008) 164–173.

[72] C.-T. Hsieh, W.-S. Fan, W.-Y. Chen, Impact of mesoporous pore distribution on adsorption of methylene blue onto titania nanotubes in aqueous solution, Microporous Mesoporous Mater. 116 (1-3) (2008) 677–683.

[73] K.-S. Lin, et al., Synthesis, characterization, and adsorption kinetics of titania nanotubes for basic dye wastewater treatment, Adsorption 16 (1-2) (2010) 47–56.

[74] N. Harsha, et al., Hydrothermal processing of hydrogen titanate/anatase-titania nanotubes and their application as strong dye-adsorbents, J. Nanosci. Nanotechnol. 11 (2) (2011) 1175–1187.